Influence on crystal nucleation of an order-disorder transition among the subcritical clusters

Richard K. Bowles [1,2,*] and Peter Harrowell [3,†]

[1]*Department of Chemistry, University of Saskatchewan, Saskatoon, SK, Canada S7H 0H1*
[2]*Centre for Quantum Topology and its Applications (quanTA), University of Saskatchewan, SK, Canada S7N 5E6*
[3]*School of Chemistry, University of Sydney, New South Wales 2006, Australia*

Studies of nucleation generally focus on the properties of the critical cluster, but the presence of defects within the crystal lattice means that the population of nuclei necessarily evolve through a distribution of precritical clusters with varying degrees of structural disorder on their way to forming a growing stable crystal. To investigate the role precritical clusters play in nucleation, we develop a simple thermodynamic model for crystal nucleation in terms of cluster size and the degree of cluster order that allows us to alter the work of forming the precritical clusters without affecting the properties of the critical cluster. The steady state and transient nucleation behavior of the system are then studied numerically, for different microscopic ordering kinetics. We find that the model exhibits a generic order-disorder transition in the precritical clusters. Independent of the types of ordering kinetics, increasing the accessibility of disordered precritical clusters decreases both the steady state nucleation rate and the nucleation lag time. Furthermore, the interplay between the free-energy surface and the microscopic ordering kinetics leads to three distinct nucleation pathways.

There is growing evidence to suggest that many systems crystallize via nonclassical nucleation where fluctuations other than that of the size of the crystal clusters play a significant mechanistic role in the phase change [1–5]. These additional fluctuations can take the form of crystalline order [1–3], cluster composition [6], or cluster shape [7], to name some common examples. A particular class of nonclassical nucleation is that involving a two-step nucleation [8–13], which has been observed in a variety of molecular [14–17] and colloidal systems [18–23]. This process, which involves the initial formation of a cluster structurally related to thermodynamically nearby metastable states that then transform to the stable state at a larger size, can be regarded as a limiting case where the fluctuations in the cluster take the form of two distinguishable states.

Previously [4,12], it has been argued that the coupling of structural fluctuations with the interfacial free energy in crystal clusters can lead, quite generically, to an order-disorder transition as a function of the cluster size. It is unclear, however, how the existence of such a transition in the precritical clusters could influence the nucleation rate. This is because the steady state value of the nucleation rate is typically regarded as being entirely determined by the kinetics at the critical nucleus [24]. This result would appear to leave only the transient nucleation rate (i.e., on the approach to steady state) to reflect the ordering process within precritical clusters. In this Letter, we show that the presence of an ordering transition gives rise to nucleation pathways reminiscent of the two-step processes and that the inclusion of the additional

accessible degrees of freedom for the crystal clusters directly changes both the transient nucleation behavior and the steady state rate.

Disorder in a crystal cluster will have two generic consequences. One will be to increase the bulk contribution to free energy of the cluster over that of the perfect crystal. The second consequence will be to decrease the crystal-liquid interfacial free energy by diminishing the entropic difference between the adjacent phases. Here, we introduce a simple model that captures these two competing effects and describes the reduced work of forming a cluster as

$$
\Delta f(n, \phi) = \frac{\Delta G(n, \phi)}{|\Delta \mu_c| k_B T} = \Delta_d (1 - \phi) n - \phi n
$$
$$
+ \gamma_c \sigma [1 - (1 - \phi) \delta] n^{2/3}, \tag{1}
$$

where ΔG is the Gibbs free energy of forming a cluster of size n, with a degree of order, ϕ, and $\Delta \mu_c$ is the difference in chemical potential between the stable equilibrium crystal phase and the metastable liquid. When $\phi = 1.0$, the cluster has the structure of the perfect crystal, but ϕ is decreased by the presence of defects characterized by a bulk excess free energy relative to that of the equilibrium crystal, $\Delta_d > 0$. While the structural nature of the defect can be interpreted broadly, it is necessarily distinct from the average order of the metastable fluid so that a cluster with $\phi = 0$ is structurally distinct from the fluid and thermodynamically unstable. The surface contributions to Δf are given by the reduced surface free energy of the perfectly ordered crystal, γ_c, the relative surface free energy decrease due to disorder, δ, and a geometric factor, σ, that accounts for the shape of the cluster.

The description of the free energy can be simplified by characterizing the free-energy landscape using the size of the

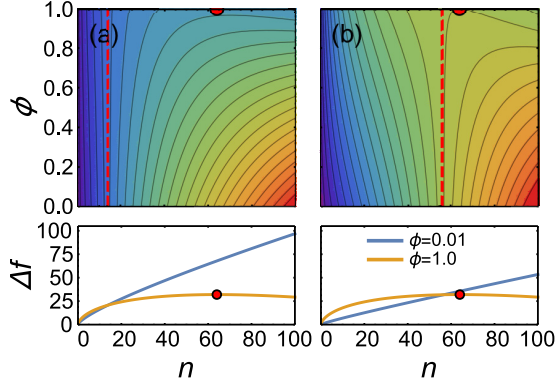*richard.bowles@usask.ca
†peter.harrowell@sydney.edu.au

FIG. 1. Free energy, $\Delta f(n, \phi)$ [Eq. (1)], using $\Delta_d = 0.4$ and $\gamma_c \sigma = 6.0$, for (a) $g = 0.40$ and (b) $g = 0.64$. Top: Contour plots of the free energy as a function n and ϕ, with $n^\dagger$ and n^* denoted by a red dashed line and red point, respectively. Bottom: Free-energy profile as a function of n for disordered clusters, $\phi = 0.01$, and ordered clusters, $\phi = 1.0$.

crossover cluster $n^\dagger$ at which the order-disorder transition occurs. At small ϕ, the free energy increases monotonically with n, indicating disordered clusters are always thermodynamically unstable with respect to cluster size and will tend to shrink. The free energy is linear in ϕ at fixed n. When a cluster is small, the slope at fixed n, $(\partial \Delta f / \partial \phi)_n$, is positive because the surface free-energy cost of forming an ordered solid-fluid interface is significantly greater than that for the disordered clusters, while the respective gain in bulk free energy is small. For larger clusters, the greater bulk free-energy gain of the ordered state begins to dominate and we see a crossover at a cluster size, $n^\dagger = (\gamma_c \sigma)^3 g^3 = \frac{27}{8} n^* g^3$, where the slope becomes negative and the ordered clusters become more stable. Here, we have introduced a characteristic dimension $g = \delta/(1 + \Delta_d)$ of the crossover cluster $n^\dagger$. Figure 1 shows the free-energy surface for different values g, along with the free-energy profiles for the growth of ordered and disordered clusters. With $\phi = 1.0$, Eq. (1) reduces the usual expression for classical nucleation theory (CNT), $\Delta G(n) = -\Delta \mu_c n + \gamma_c \sigma n^{2/3}$, going through a maximum at the critical size $n^* = 8(\gamma_c \sigma)^3/27$, and is independent of g.

For $g \leqslant 2/3$, $n^\dagger$ occurs before n^*, which is independent of g, and the lowest free-energy path for nucleation involves the initial growth of small disordered clusters that then order at $n^\dagger$ to form a perfectly ordered cluster before eventually going over the nucleation barrier [Figs. 1(a) and 1(b)]. Phenomenologically, the model is similar to two-step nucleation models where the intermediate metastable phase is higher in free energy than the mother phase and has low surface tension [9,13], but the defects included here cannot form a bulk thermodynamic phase so the clusters remain thermodynamically unstable and the key features of the model should be generally applicable to crystal nucleation. For $g \geqslant 2/3$, n^* begins to grow and become more disordered and $n^\dagger = n^*$. We focus on cases with $n^\dagger < n^*$.

The kinetic evolution of clusters on this free-energy surface can be characterized in terms of equilibrium reactions for the growth and decay of a cluster through the addition or loss of a monomer and for the order-disorder processes. The rate

constants for the growth and decay processes, obtained from a simple rate theory, are given by [24–26]

$$\kappa_{n,\phi}^+ = n^{2/3} \exp[-\Delta_n G(n, \phi)/2k_B T],$$

$$\kappa_{n,\phi}^- = (n-1)^{2/3} \exp[\Delta_n G(n-1, \phi)/2k_B T], \quad (2)$$

where $\Delta_n G(n, \phi) = \Delta G(n + 1, \phi) - \Delta G(n, \phi)$ and the prefactor accounts for the addition and loss of monomers at the surface. Similarly, the rate constants for the order-disorder kinetics are

$$\omega_{n,\phi}^+ = \alpha(n) \exp[-\Delta_\phi G(n, \phi)/2k_B T],$$

$$\omega_{n,\phi}^- = \alpha(n) \exp[\Delta_\phi G(n, \phi - \Delta \phi)/2k_B T], \quad (3)$$

where $\Delta_\phi G(n, \phi) = \Delta G(n, \phi + \Delta \phi) - \Delta G(n, \phi)$, and $\alpha(n)$ is a size-dependent prefactor that captures the effects of different ordering mechanisms. The ordering kinetics in a cluster will depend both on the relationship between the equilibrium crystal order and the local structure of the defect, and where structural relaxation can occur. The crystal-fluid interface at the cluster surface is the most dynamic region of a cluster, where annealing can occur. If the defects structure is incompatible with the crystal structure, the defect must diffuse to the surface before rearranging in a surface-mediated ordering (SMO) process, then $\alpha(n) \sim D/n^{2/3}$, where the size dependence accounts for the additional time it takes for a defect to reach the surface in larger clusters and D is the defect diffusion coefficient. As an alternative, we assume a uniform ordering (UO) process, where the defects can easily rearrange without diffusion, has kinetics determined by the free-energy surface alone and $\alpha(n) = C$ is the size-independent constant.

The time-dependent forward rates of cluster growth and cluster ordering can be defined for n, ϕ clusters as

$$I_{n,\phi,t}^g = \kappa_{n,\phi}^+ N_{n,\phi,t} - \kappa_{n+1,\phi}^- N_{n+1,\phi,t},$$

$$I_{n,\phi,t}^o = \omega_{n,\phi}^+ N_{n,\phi,t} - \omega_{n,\phi+\delta\phi}^- N_{n,\phi+\delta\phi,t}, \quad (4)$$

respectively, where $N_{n,\phi,t}$ is the number of clusters with size and order n, ϕ at time t. The time evolution of the cluster population can then be described by $\frac{\partial N_{n,\phi,t}}{\partial t} = I_{n-1,\phi,t}^g - I_{n,\phi,t}^g + I_{n,\phi-\delta\phi,t}^o - I_{n,\phi,t}^o$, which we solve numerically using discrete time intervals, δt, following a method developed by Kelton *et al.* [26]. Full details of the numerical method can be found in the Supplemental Material (SM) [27].

The steady state population of clusters, $N_{n,\phi,ss}$, obtained at $t \approx 3000$ s, is solely a function of the free-energy surface and is the same for both kinetic models. Figure 2(a) shows that $N_{n,\phi,ss}$ for the ordered clusters exhibits a decay consistent with the expectations for the steady state population from a CNT free-energy model. At $\phi = 1.0$, $\Delta f(n, \phi)$ is independent of g, so the small decrease in the steady state population at the transition state as g increases is the result of changes in the free energy at other points on the surface. However, increasing g directly lowers $\Delta f(n, \phi)$ for the disordered clusters, making these states more accessible, and causing $N_{n,\phi,ss}$ to increase by many orders of magnitude. Figure 2(b) shows the large excess of disordered clusters relative to ordered clusters for intermediate cluster sizes.

We measure the steady state forward growth rate through the critical cluster, $I_{n^*,\phi^*,ss}^g$, and because the two-dimensional nature of free-energy surface means clusters can nucleate
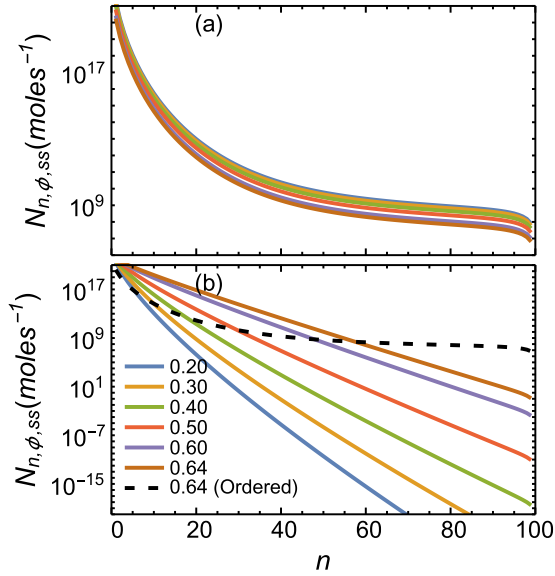
FIG. 2. Steady state cluster populations, $N_{n,\phi,ss}$, as a function of n in the surface-mediated ordering model with different values of g for (a) ordered clusters, $\phi = 1.0$, and (b) disordered clusters, $\phi = 0.01$. The dashed line represents the ordered cluster for comparison.

without passing through the critical cluster, we also measure the total steady state forward rate entering the free-energy crystal basin, $I^c_{n,\phi,ss}$, where, for simplicity, the crystal basin is defined as the rectangular region $n > n^*$, $\phi > 0.9$. Figure 3(a) shows that $I^g_{n^*,\phi^*,ss}$ and $I^c_{n,\phi,ss}$ decrease by factors of approximately 10 and 2, respectively, as g increases. The effect is independent of the nature of the microscopic kinetics, although there is a small but growing difference in $I^c_{n,\phi,ss}$
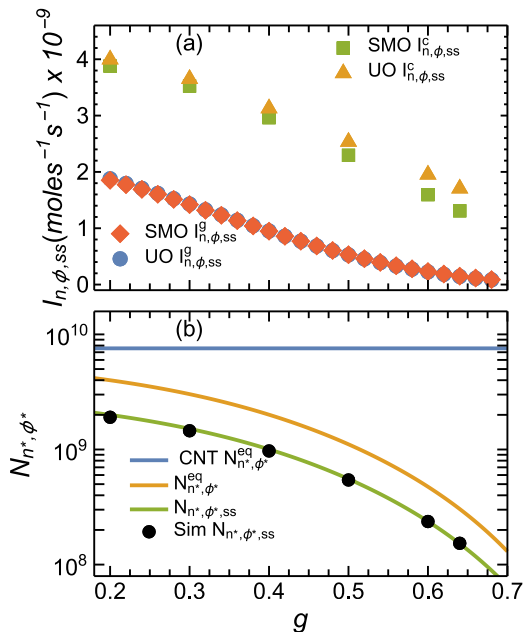

FIG. 3. (a) ($I^g_{n^*,\phi^*,ss}$ and $I^c_{n,\phi,ss}$ as a function of g for SMO and UO microscopic ordering kinetics. (b) CNT, equilibrium, and steady state cluster populations obtained from Eq. (5) compared to the numerical simulation steady state.
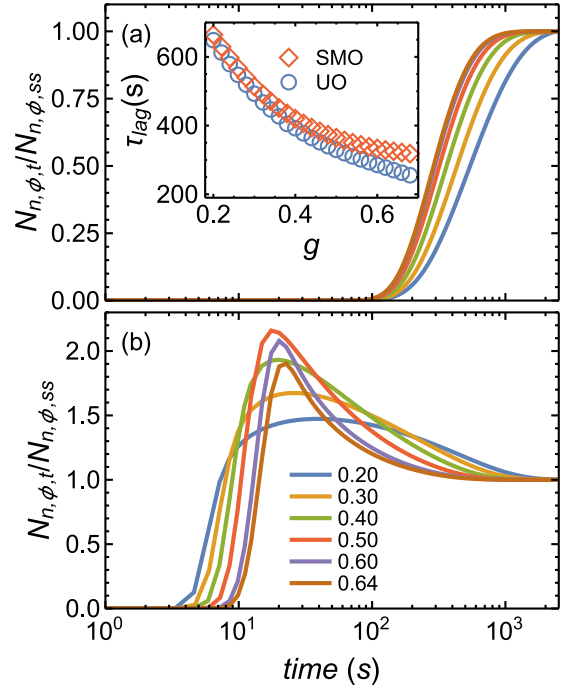

FIG. 4. Relative transient cluster populations for $n = 64$ sized clusters as a function of time in the SMO model with different values of g (similar results for the UO model not shown). (a) Ordered clusters $\phi = 1.0$. Inset shows τ_{lag} as a function of g for uniform and surface-mediated ordering. (b) Disordered clusters $\phi = 0.01$.

for the SMO and UO kinetics at large g, which suggests it arises from the changes in the free-energy surface and the accompanying increase in the accessibility of the disordered cluster states. One way to understand the rate decrease is to note that the increased number of precritical clusters reduces the liquid monomers available for cluster formation. The equilibrium number of critical clusters is given by (see SM for derivation)

$$N^{eq}_{n^*,\phi^*} = N_0 \exp[-\beta \Delta G(n^*, \phi^*)], \tag{5}$$

where $N_0 = N/(1 + \sum_{n=1}^{n^*} n \int_0^1 \exp[-\beta \Delta G(n, \phi) d\phi])$ is the number of liquid monomers. The steady state cluster population is obtained as $N_{n^*,\phi^*,ss} \approx N^{eq}_{n^*,\phi^*}/2$ [24]. Figure 3(b) shows Eq. (5) accurately predicts $N_{n^*,\phi^*,ss}$. As g increases, making the disorder clusters more accessible, the integral over $\exp[-\beta \Delta G(n, \phi)]$ increases, leading to a decrease in N_0, while the equilibrium number of clusters predicted by CNT remains constant. Increasing the accessibility of the disordered cluster states also influences the transient nucleation behavior, with Fig. 4(a) showing that the transient cluster population, relative to steady state value, for the critical cluster grows at earlier times for larger g, leading to lower lag times, τ_{lag} (see inset). To understand this, we follow the transient cluster populations of the disordered clusters as a function time. Figure 4(b) shows that $N_{n,\phi,t}$ for large disordered clusters in the SMO model actually overshoot their steady state populations at times an order of magnitude earlier than the critical clusters, then decay towards the steady state at longer timescales. However, for $g = 0.2$ these large disordered populations are very small and the cluster population is restricted to
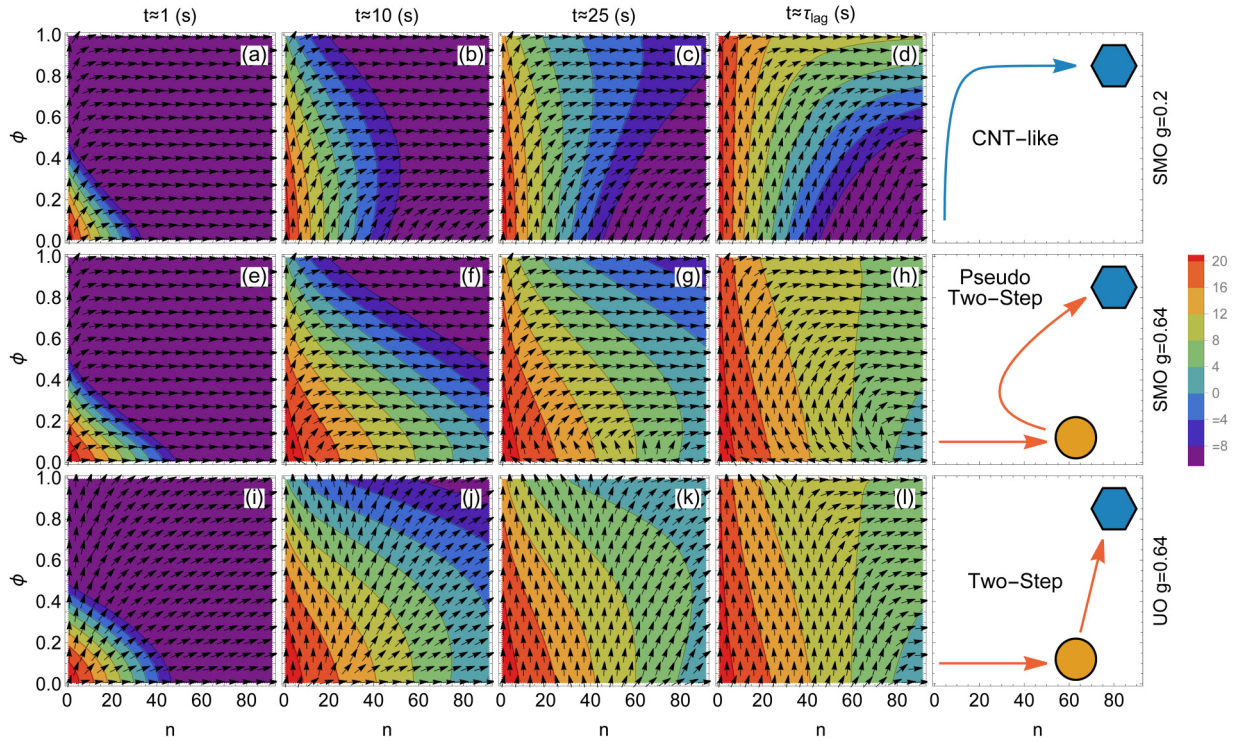
FIG. 5. Contour plots showing $\ln N_{n,\phi,t}$ and vector plots of the forward rates for (a)–(d) SMO with $g = 0.2$, (e)–(h) SMO with $g = 0.64$, and (i)–(l) UO with $g = 0.64$, at times $t \approx 1, \ 10,$ and 25 s and $\tau_{\rm lag}$ for coulombs, left to right, respectively. The vector components, $I^g_{n,\phi,t}$ and $I^o_{n,\phi,t}$, are normalized relative to $|I_{n,\phi,t}| = \sqrt{(I^g_{n,\phi,t})^2 + (I^o_{n,\phi,t})^2}$.

a narrow channel for small disorder clusters, so clusters order before they grow [Figs. 5(a)–5(d)] in a CNT-like process. With $g = 0.64$, large excess populations of disordered clusters form at early times that then flow on to other regions of the free-energy surface through an increased number of accessible cluster states [Figs. 5(e)–5(h)] to decrease $\tau_{\rm lag}$.

Figure 5 also highlights the interplay between the free-energy surface and the microscopic kinetics in determining the nature of the nucleation mechanism, which in the present system yields the three nucleation pathways. With $g = 0.2$, both the SMO [Figs. 5(a)–5(d)] and UO models exhibit the same CNT-like nucleation mechanism because both the free-energy surface and the microscopic kinetics of the SMO model favor ordering at small clusters. When $g = 0.64$, the free-energy surface favors formation of large disordered clusters, and we see large populations of disordered clusters form at early times, but the subsequent evolution of the clusters is determined by the microscopic kinetics. The ordering kinetics is suppressed for larger disordered clusters in the SMO model because defects must diffuse to the surface before they can rearrange to the stable state. As a result, we see a pseudo-two-step nucleation pathway [Figs. 5(e)–5(h)] where the large disordered clusters do not play a role as direct intermediates and the growth rate, $I^g_{n,\phi,t}$, for these disordered clusters becomes negative as the clusters shrink to smaller sizes before ordering. In contrast, the ordering process for the large disordered clusters in the UO model is determined by the free-energy surface, which is downhill for $n > n^\dagger$, and the large disordered cluster tends to order directly towards

crystal in a two-step nucleation process. The more direct route over the free-energy surface for the disordered clusters in the UO model may also account for the model's shorter lag times compared to those in the SMO model.

The results presented here have been obtained from the simple model defined in Eq. (1). While we have argued that the reported behavior is generic, it would be useful to confirm this with treatment of nucleation based on a more explicit model that covers a broader range of nucleation phenomena. Iwamatsu [9] models two-step nucleation, where nucleation proceeds through the initial formation of clusters of a metastable intermediate phase, as a core-shell nuclei with the metastable state wetting the stable phase core so that the mole fraction of the stable state in the cluster, or the size of the core, becomes an additional degree of freedom. The model exhibits a phase transition from a cluster rich in the metastable state to a cluster dominated by the stable state at a particular $n^\dagger$, similar to the order-disorder transition observed in our model, and has been shown to provide an accurate description of the nucleation process in an Ising model with nearest and next-nearest interactions [12]. In the SM, we examine the nucleation properties of the Iwamatsu model in two case studies, including its application to the lattice model of Poole *et al.* (see Figs. S4–S8). As the stability of the intermediate phase (g in our model) is increased, making the disordered clusters more accessible, there is a decrease in N_0 and the number of equilibrium critical clusters. This is the same effect observed for our model in Fig. 3(b). However, in the Iwamatsu model, the thermodynamic state of the system begins to

directly influence the properties of the critical nucleus causing the model free energy to decrease. The equilibrium number of critical clusters, which ultimately gives the nucleation rate, then includes competing contributions from the expanding metastable basin and the decreasing free energy of the critical nucleus [28,29]. Furthermore, a recent numerical study [30] of two-step vapor-crystal condensation in water, below the triple point, exhibits transient nucleation behavior similar to that observed here in Figs. 5(i)–5(l).

In conclusion, we have shown that the inclusion of additional order parameter(s) describing the clusters coupled with a free energy that promotes the sampling of this expanded configuration space will produce, quite generally, a reduction in the steady state nucleation rate by reducing the amount of available monomer. Here, we only included one defect type. Increasing the number of different types of defects and disorder available to the crystal would expand the number of available precritical states, which could lead to further slowing of the nucleation rate that has implications for the glass forming ability of a material. Beyond this generic impact, we have shown how the details of the ordering kinetics in the subcritical clusters can significantly alter the transient nucleation kinetics. This is of particular importance in the analysis of molecular dynamics simulations of crystal nucleation where the transients will dominate over the accessible observation time. Furthermore, while large disordered clusters have been observed, for example in protein crystallization [31,32], its not clear if they are directly involved in the nucleation pathway [33–35]. Our work suggests that the nature of the microscopic growth and ordering kinetics might provide insight into the role these large disordered clusters play in nucleation.

[1] P. R. ten Wolde and D. Frenkel, Enhancement of protein crystal nucleation by critical density fluctuations, Science **277**, 1975 (1997).

[2] V. Talanquer and D. W. Oxtoby, Crystal nucleation in the presence of a metastable critical point, J. Chem. Phys. **109**, 223 (1998).

[3] S. Whitelam, Nonclassical assembly pathways of anisotropic particles, J. Chem. Phys. **132**, 194901 (2010).

[4] P. Harrowell, On the existence of a structural instability in subcritical crystalline fluctuations in a supercooled liquid, J. Phys.: Condens. Matter **22**, 364106 (2010).

[5] J. F. Lutsko, How crystals form: A theory of nucleation pathways, Sci. Adv. **5**, eaav7399 (2019).

[6] F. Ito, Y. Suzuki, J.-i. Fujimori, T. Sagawa, M. Hara, T. Seki, R. Yasukuni, and M. L. de la Chapelle, Direct visualization of the two-step nucleation model by fluorescence color changes during evaporative crystallization from solution, Sci. Rep. **6**, 22918 (2016).

[7] H. H. Pang, Q. L. Bi, H. S. Huang, and Y. J. Lü, Anisotropic stress inhibits crystallization in Cu-Zr glass-forming liquids, J. Chem. Phys. **147**, 234503 (2017).

[8] N. Duff and B. Peters, Nucleation in a Potts lattice gas model of crystallization from solution, J. Chem. Phys. **131**, 184101 (2009).

[9] M. Iwamatsu, Free-energy landscape of nucleation with an intermediate metastable phase studied using capillary approximation, J. Chem. Phys. **134**, 164508 (2011).

[10] L. O. Hedges and S. Whitelam, Patterning a surface so as to speed nucleation from solution, Soft Matter **8**, 8624 (2012).

[11] S. M. A. Malek, G. P. Morrow, and I. Saika-Voivod, Crystallization of Lennard-Jones nanodroplets: From near melting to deeply supercooled, J. Chem. Phys. **142**, 124506 (2015).

[12] D. James, S. Beairsto, C. Hartt, O. Zavalov, I. Saika-Voivod, R. K. Bowles, and P. H. Poole, Phase transitions in fluctuations and their role in two-step nucleation, J. Chem. Phys. **150**, 074501 (2019).

[13] D. Eaton, I. Saika-Voivod, R. K. Bowles, and P. H. Poole, Free energy surface of two-step nucleation, J. Chem. Phys. **154**, 234507 (2021).

[14] D. Gebauer, A. Völkel, and H. Cölfen, Stable prenucleation calcium carbonate clusters, Science **322**, 1819 (2008).

[15] R. P. Sear, The non-classical nucleation of crystals: microscopic mechanisms and applications to molecular crystals, ice and calcium carbonate, Int. Mater. Rev. **57**, 328 (2012).

[16] S. Ishizuka, Y. Kimura, T. Yamazaki, T. Hama, N. Watanabe, and A. Kouchi, Two-step process in homogeneous nucleation of alumina in supersaturated vapor, Chem. Mater. **28**, 8732 (2016).

[17] A. Kumar and V. Molinero, Two-step to one-step nucleation of a zeolite through a metastable gyroid mesophase, J. Phys. Chem. Lett. **9**, 5692 (2018).

[18] J. R. Savage and A. D. Dinsmore, Experimental Evidence for Two-Step Nucleation in Colloidal Crystallization, Phys. Rev. Lett. **102**, 198302 (2009).

[19] P. Tan, N. Xu, and L. Xu, Visualizing kinetic pathways of homogeneous nucleation in colloidal crystallization, Nat. Phys. **10**, 73 (2014).

[20] T. K. Haxton, L. O. Hedges, and S. Whitelam, Crystallization and arrest mechanisms of model colloids, Soft Matter **11**, 9307 (2015).

[21] Y. Peng, F. Wang, Z. Wang, A. M. Alsayed, Z. Zhang, A. G. Yodh, and Y. Han, Two-step nucleation mechanism in solid-solid phase transitions, Nat. Mater. **14**, 101 (2015).

[22] W. Qi, Y. Peng, Y. Han, R. K. Bowles, and M. Dijkstra, Nonclassical Nucleation in a Solid-Solid Transition of Confined Hard Spheres, Phys. Rev. Lett. **115**, 185701 (2015).

[23] S. Lee, E. G. Teich, M. Engel, and S. C. Glotzer, Entropic colloidal crystallization pathways via fluid-fluid transitions and multidimensional prenucleation motifs, Proc. Natl. Acad. Sci. USA **116**, 14843 (2019).

[24] K. Kelton and A. Greer, *Nucleation in Condensed Matter: Applications in Materials and Biology* (Elsevier, New York, 2010), Vol. 15.

[25] D. Turnbull and J. C. Fisher, Rate of nucleation in condensed systems, J. Chem. Phys. **17**, 71 (1949).

[26] K. F. Kelton, A. L. Greer, and C. V. Thompson, Transient nucleation in condensed systems, J. Chem. Phys. **79**, 6261 (1983).

[27] See Supplemental Material at http://link.aps.org/supplemental/10.1103/PhysRevE.105.L062602 for additional methods and analysis.

[28] B. Scheifele, I. Saika-Voivod, R. K. Bowles, and P. H. Poole, Heterogeneous nucleation in the low-barrier regime, Phys. Rev. E **87**, 042407 (2013).

[29] C. C. Asuquo, D. McArthur, and R. K. Bowles, Competitive heterogeneous nucleation onto a microscopic impurity in a Potts model, J. Chem. Phys. **145**, 064511 (2016).

[30] S. Auer and D. Kashchiev, Two-step crystal nucleation kinetics: Solution of the master equation, J. Cryst. Growth **580**, 126469 (2022).

[31] P. G. Vekilov, The two-step mechanism of nucleation of crystals in solution, Nanoscale **2**, 2346 (2010).

[32] F. Zhang, Nonclassical nucleation pathways in protein crystallization, J. Phys.: Condens. Matter **29**, 443002 (2017).

[33] L. Houben, H. Weissman, S. G. Wolf, and B. Rybtchinski, A mechanism of ferritin crystallization revealed by cryo-STEM tomography, Nature (London) **579**, 540 (2020).

[34] T. Yamazaki, Y. Kimura, P. G. Vekilov, E. Furukawa, M. Shirai, H. Matsumoto, A. E. S. V. Driessche, and K. Tsukamoto, Two types of amorphous protein particles facilitate crystal nucleation, Proc. Natl. Acad. Sci. USA **114**, 2154 (2017).

[35] M. Sleutel and A. E. S. V. Driessche, Nucleation of protein crystals— a nanoscopic perspective, Nanoscale **10**, 12256 (2018).